

Letters

Unifying the Transformer Current in Multiple Phase Modulation Without Current Spike During Load Transients

Yu Yan , Hua Bai , Ruirui Chen , Leon M. Tolbert , and Fred Wang

Abstract—To accelerate the dynamic response in a dual active bridge converter, feed-forward control can be applied in parallel to the conventional PI controller for closed-loop control. The transformer current thus changes significantly due to the phase shift change. A current spike can appear during load transients, particularly when using multiple phase shift modulation. Effort has been made in the previous literature to implement active compensation between two different steady-state operations to eliminate the transformer current spike; however, this results in a complicated control structure. This letter thus proposes a novel modulation method unifying the transformer current for dual phase shift and triple phase shift modulation to mitigate the transformer current spike when switching among various phase shift controls during load transients. By applying the proposed pulsewidth modulation strategy, the instantaneous value of the transformer current stays the same at the beginning of the switching period even with different steady-state modulation techniques. Also, full-operation-range zero-voltage switching can be realized for the primary side or the secondary side switches by combining with the proposed modulation strategy. An experimental prototype demonstration validates the proposed modulation strategy.

Index Terms—Current spike elimination, dual active bridges (DABs), multiple phase shift (MPS), zero-voltage switching (ZVS).

I. INTRODUCTION

A DUAL active bridge (DAB) converter is an excellent topology owing to its galvanic isolation, adjustable voltage gains, and bidirectional power flow [1] in Fig. 1. DAB has attractive features, such as high power density and high efficiency, by applying high switching frequency to drive the active switches while also realizing soft switching. To further improve the performance of the DAB converter, different modulation strategies have been developed, such as dual phase shift (DPS)

Manuscript received 1 June 2022; revised 6 July 2022; accepted 2 August 2022. Date of publication 15 August 2022; date of current version 6 September 2022. This work was supported by the Advanced Manufacturing Office, United States Department of Energy under Award DE-EE0009134. (Corresponding author: Yu Yan.)

Yu Yan, Hua Bai, Ruirui Chen, and Leon M. Tolbert are with the Department of Electrical Engineering and Computer Science, The University of Tennessee Knoxville, Knoxville, TN 37996 USA (e-mail: yyan15@vols.utk.edu; kevin-bai@icloud.com; rchen14@vols.utk.edu; tolbert@utk.edu).

Fred Wang is with the Department of Electrical Engineering and Computer Science, The University of Tennessee, Knoxville, TN 37830 USA (e-mail: fred.wang@utk.edu).

Color versions of one or more figures in this article are available at <https://doi.org/10.1109/TPEL.2022.3198498>.

Digital Object Identifier 10.1109/TPEL.2022.3198498

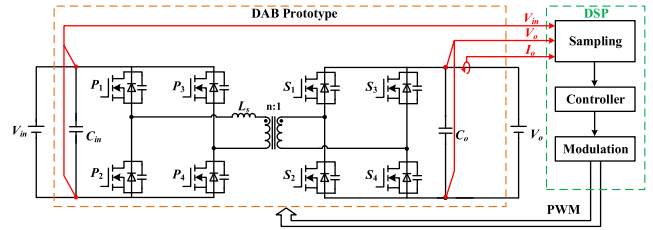


Fig. 1. Topology of DAB converter with digital control.

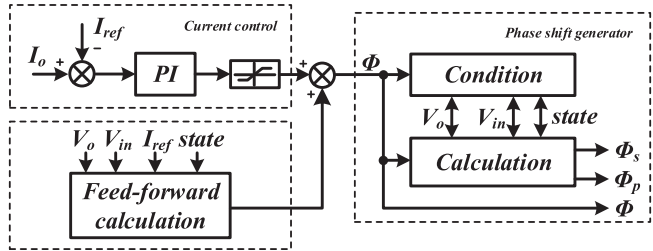


Fig. 2. Structure of the closed-loop control in the DAB converter.

modulation, triple phase shift (TPS) modulation, and multiple phase shift (MPS) modulation [2], [3], [4]. Most of the newly proposed modulation strategies only focused on steady-state performance, such as securing zero-voltage switching (ZVS) [5] and reducing the transformer current rms, instead of the issues during transient states.

A typical application of the DAB converter is to serve as the interface between a high-voltage and a low-voltage dc bus. While the low-voltage bus can be a dc microgrid connected to different types of loads (motor drive or resistive load), an energy source, or energy storage device, it also can feed the high-voltage dc bus when necessary. For medium-voltage devices for grid applications (10-kV device), the switching loss is much higher than that in lower voltage SiC devices (1700 V) [6], which means ZVS for medium-voltage device is necessary.

The DAB converter should have a fast dynamic response to meet electric grid codes in load transients; however, this fast switching can cause issues, such as current spikes, in the transformer that can damage the semiconductor devices. The root of this issue is the abrupt change of phase shift thus transformer current waveform, as described in the previous literature [7].

Some active compensation methods were discussed to mitigate the transformer current change by modifying the duty cycle of certain switches in the next switching cycle compared to the previous cycle during the phase shift change [7], [8], [9]. Hu et al. [10] and Wei et al. [11] also provided solutions for the magnetizing dc bias during a load transient by providing active compensation. Such active compensation during the transients, however, can make the control complicated when applying MPS modulation to cover wide voltage and power range. Because the transformer currents are independent in each modulation mode, the compensation method has to consider all transitions among all modulation modes. Also, a zero current in performance optimization of a high current DAB with a wide operating voltage range or triangular modulation control [4], [12] can also be utilized in the current spike elimination method, which means there is no current difference at the beginning of the switching cycle.

In this letter, a novel modulation strategy is proposed with the unified transformer current in DPS and TPS modulation, which not only is designed for steady-state operation but also considers current spikes during a load transient. With the application of the proposed modulation, there is no need to consider the active compensation between DPS and TPS, which simplifies the compensation over the whole operation range. At the same time, the primary switches can operate with ZVS thus eliminating their switching loss. In Section II, the root cause of the transformer current spike during a load transient is analyzed. Then, a modulation strategy design is proposed to unify the transformer current control in DPS and TPS modulation in Section III. The mitigation of the transformer current spike in the whole operation range is provided in Section IV. Section V contains the experimental results to validate the proposed modulation strategy.

II. ROOT CAUSE OF THE CURRENT SPIKE IN TRANSFORMER

The output current of the DAB converter is regulated by the phase shift between the primary-side and secondary-side H-bridges. When a load current transient happens, to track the reference current, the phase shift needs to change swiftly. To accelerate the dynamic response, feed-forward control is commonly applied in parallel with a PI controller, tracking the reference current as shown in Fig. 2. Fig. 3 shows an example for closed-loop control for the DAB converter. With the MPS modulation, the phase shift between the primary side and the secondary side determines the inner phase shifts associated with the input voltage and the output voltage [2]. In Fig. 3, ϕ is the phase shift between the primary side and the secondary side, ϕ_s is the secondary-side inner phase shift, and ϕ_p is the primary-side inner phase shift, which is marked in Fig. 3. The first half bridge at the primary side is set as the reference leg when defining the phase shifts.

A simulation example of the load current transient is provided in Fig. 4. The simulation parameters are shown in Table I, which is also the test condition for the control algorithm in the laboratory. To verify the proposed modulation strategy, the

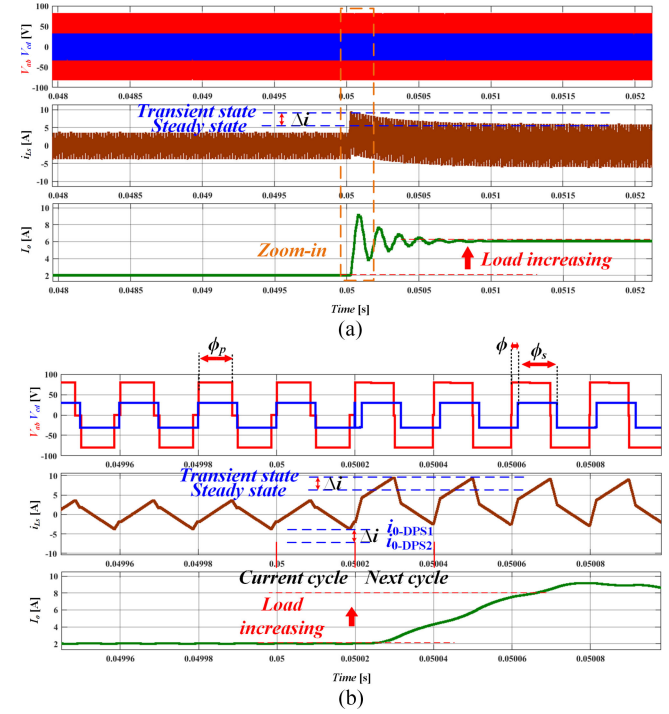


Fig. 3. Simulation waveforms during load transients. (a) Load current increasing with the current spike of the transformer. (b) Zoomed-in waveforms.

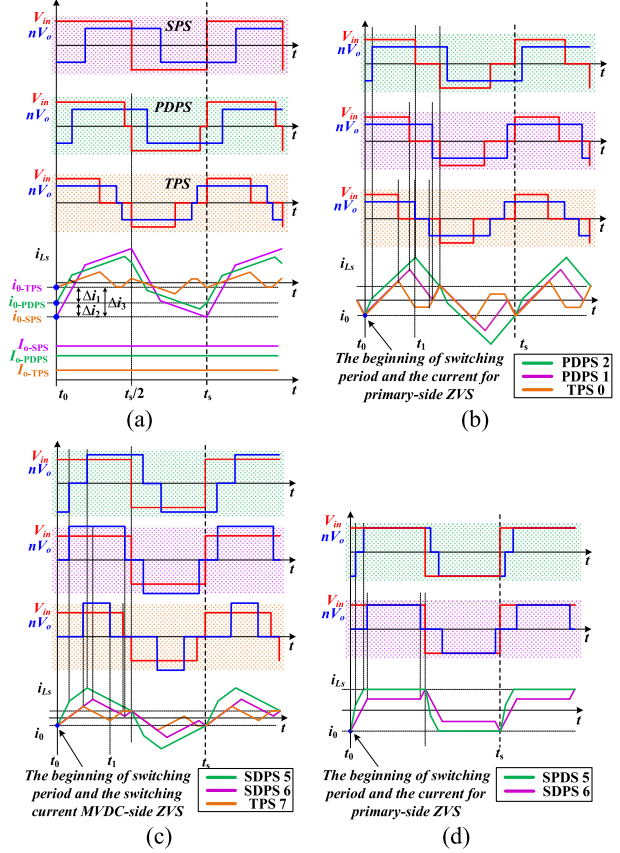


Fig. 4. Switching waveforms of the proposed modulation strategies. (a) Modulations without the unified switching current. (b) PDPS and TPS when $V_{\text{in}} > nV_o$. (c) SDPS and TPS when $V_{\text{in}} < nV_o$. (d) SDPS when $V_{\text{in}} = nV_o$.

TABLE I
PROTOTYPE SETUP

Parameter	Value	Parameter	Value
Input voltage	80 V	Turns ratio	2
Output Voltage	30~50 V	Inductance	36 μ H
Switching frequency	50 kHz	--	--

experiments are adopted at low voltage condition. During the load current change, the reference current increases. A new phase shift will be uploaded to the DAB converter in the next switching cycle. Under light load, TPS modulation is applied to ensure ZVS and reduce the reactive power. At medium load, DPS modulation is adopted. During the transition between TPS and DPS when the load current increases, the current spike appears in the transformer.

If the switching currents at the beginning of the switching period under different conditions have the same constraints, there will be no transformer current spike even when phase shifts change dramatically. When the load transient happens between the TPS and DPS modulation, there is no need for the additional active compensation. Considering the load transient between SPS and other modulations, because of the unified switching current of DPS and TPS, other modulations can be regarded as a single pattern to be compensated. Otherwise, according to the previous literature, the current spike elimination methods need to be considered between each modulation or even within a single modulation. Thus, the controller design can be simplified with the proposed modulation strategies.

The cause of the transformer current spike is the continuity of the transformer current and the discontinuous phase shift. When a new phase shift is applied to switches at a certain point of the switching cycle, it is set by the microcontrol unit. When applying the different modulations, as shown in Fig. 5(a), the transformer current at the beginning of the switching period is provided in (1), and the current difference is listed in (2). The switching current of SPS modulation is only related to the phase shift between the primary side and the secondary side. On the other hand, because of the additional inner phase shifts, DPS and TPS modulation have more flexible and variable switching current, which offer more degrees of freedom to shape the transformer current

$$\begin{cases} i_{0_SPS} = -\frac{V_{in}+nV_o(2\phi-1)}{4L_s f_s} \\ i_{0_PDPS} = -\frac{V_{in}\phi_p+nV_o(2\phi-1)}{4L_s f_s} \\ i_{0_TPS} = -\frac{V_{in}\phi_p-nV_o(\phi+\phi_s)}{4L_s f_s} \end{cases} \quad (1)$$

$$\begin{cases} \Delta i_1 = \frac{nV_o(3\phi+\phi_s-1)}{4L_s f_s} \\ \Delta i_2 = \frac{V_{in}(1-\phi_p)}{4L_s f_s} \\ \Delta i_3 = \frac{V_{in}(1-\phi_p)+nV_o(3\phi+\phi_s-1)}{4L_s f_s} \end{cases} \quad (2)$$

III. UNIFIED TRANSFORMER CURRENT IN MULTIPLE PHASE MODULATION

As mentioned earlier, the transformer current at a certain switching point in DPS and TPS modulation can be unified

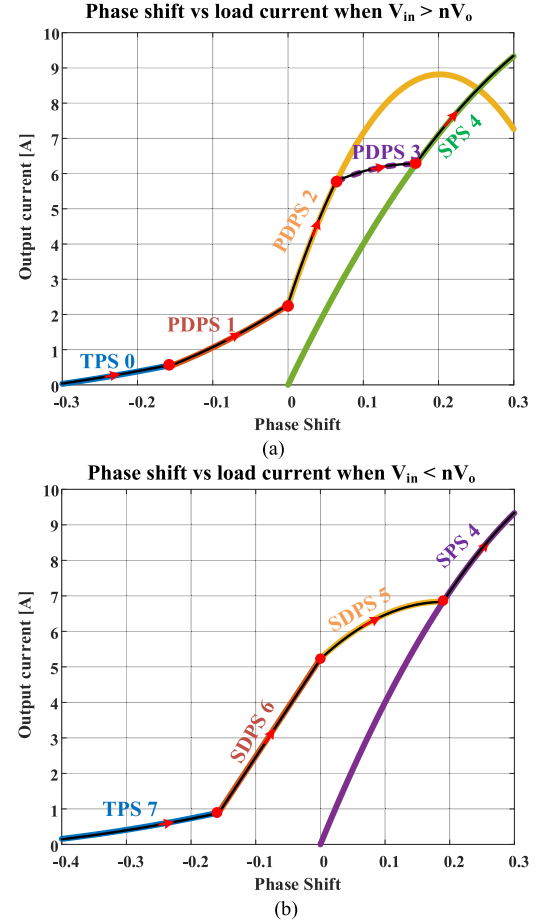


Fig. 5. Example of phase shift versus output current. (a) Modulations when $V_{in} > nV_o$ ($V_{in} = 80$ V, $nV_o = 60$ V). (b) Modulations when $V_{in} < nV_o$ ($V_{in} = 80$ V, $nV_o = 100$ V).

by adjusting the inner phase shifts. This switching current can stay the same under different load conditions and modulations. Meanwhile, if the selected switching action corresponds with the primary-side switches and if the value of the current setting is large enough, it can also realize ZVS for the primary side for the full load range. By following this theory, the designed modulation strategies are shown in Fig. 6.

To fulfill the minimum initial current to realize ZVS for the primary-side switches under different modulations, the transformer current at t_0 should be

$$I_{ZVS0}(V_o) \geq \sqrt{\frac{4Q_{oss}(V_{in})nV_o}{L_s}}. \quad (3)$$

When the input voltage is higher than the reflected output current, to unify the switching current in different modulations, the transformer current at the beginning of the switching period should be the same in (4)

$$i_{0_PDPS} = i_{0_TPS0} = I_{ZVS0}(V_o). \quad (4)$$

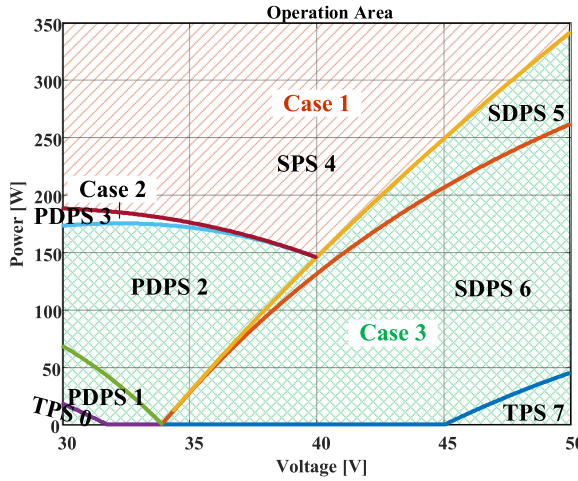


Fig. 6. Operational area for different modulations.

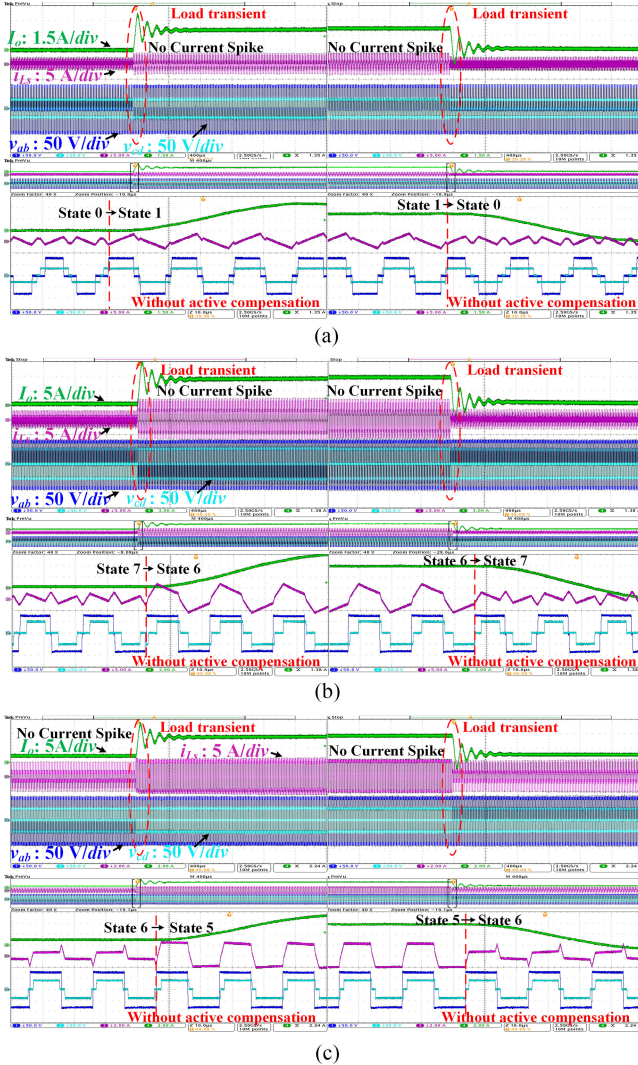


Fig. 7. Experiment waveforms during load transient. (a) TPS0 to PDPS1 without active compensation. (b) TPS7 to SDPS5 without active compensation. (c) SDPS6 to SDPS5 without active compensation.

The primary-side inner phase shift in DPS modulation is derived in (5), according to (1) and (4)

$$\begin{cases} \text{PDPS1}(\phi < 0) : \phi_p = \frac{4L_s f_s I_{ZVS0} + nV_o(1+2\phi)}{V_{in}} \\ \text{PDPS2}(\phi \geq 0) : \phi_p = \frac{4L_s f_s I_{ZVS0} + nV_o(1-2\phi)}{V_{in}} \end{cases}. \quad (5)$$

At light load, to realize ZVS for the secondary-side switches, the transformer current at t_1 should meet the minimum required value to finish the ZVS transition [5]. Hence, the inner phase shift can be further derived in (6). The switching waveform of the designed modulations is shown in Fig. 5(b)

$$\text{TPS0} : \begin{cases} \phi_p = \frac{nV_o(1+D) + 2L_s f_s (I_{ZVS0} - I_{ZVS,t1})}{V_{in}} \\ \phi_s = \frac{nV_o - 2L_s f_s (I_{ZVS0} + I_{ZVS,t1})}{nV_o} \end{cases}. \quad (6)$$

The relationship between the phase shift and the output current for different modulation methods is plotted in Fig. 6(a). But with the increasing phase shift, the output current is not monotonic in PDPS2 before switching to SPS modulation. An additional DPS modulation is then designed to realize a seamless transition between primary-side dual phase shift (PDPS) and SPS modulation in (7). As shown in Fig. 6(a), the dashed line represents the DPS modulation designed for a seamless transition

$$\text{PDPS3} : \phi_p = \frac{2V_{in}\phi + nV_o - 4L_s f_s I_{ZVS}}{V_{in}}. \quad (7)$$

When the input voltage is lower than the reflected output voltage, the inner phase is inserted at the secondary-side switches. The switching waveforms are shown in Fig. 4(c). To unify the transformer current at the beginning of the switching period, the inner phase shift at the secondary-side H-bridge in secondary-side dual phase shift (SDPS) modulation is

$$\begin{cases} \text{SDPS5}(\phi \geq 0) : \phi_s = \frac{4L_s f_s I_{ZVS0} + nV_o(2-\phi) - V_{in}}{nV_o} \\ \text{SDPS6}(\phi < 0) : \phi_s = \frac{4L_s f_s I_{ZVS0} + nV_o(2+\phi) - V_{in}}{nV_o} \end{cases}. \quad (8)$$

In TPS modulation, to realize ZVS for secondary-side switches, the switching current at t_1 should also be large enough to finish the ZVS transition. To meet the requirements of the unified transformer current and the ZVS current, the inner phase shifts are

$$\text{TPS7} : \begin{cases} \phi_p = \frac{V_{iu}(1+\phi) + 2L_s f_s (I_{ZVS0} + I_{ZVS,t1})}{V_{in}} \\ \phi_s = 2 + \phi + \frac{2L_s f_s (I_{ZVS0} - I_{ZVS,t1}) - V_{in}(1+\phi)}{nV_o} \end{cases}. \quad (9)$$

The relationship between the phase shift and output current is shown in Fig. 6(b) among TPS, SDPS, and SPS modulations. The proposed modulations with the unified transformer current can operate under different voltage gains and load conditions.

By implementing the proposed modulation strategy, there is no current spike during the load current transient when using DPS and TPS modulation. But the switching current of SPS modulation is solely decided by the load without additional flexible inner phase shifts. Further current spike elimination, including SPS, needs to be considered. Owing to the unified switching current by the proposed modulation, the transformer current is the same under different DPS and TPS, which can be

integrated as a single pattern when designing active compensation.

Fig. 6 shows the distribution of the different modulation strategies. Case 1 is the operational area with SPS. Case 2 is the operational area with PDPS3 used for a seamless transition in a steady state. Also, by applying PDPS3, ZVS for the secondary-side switches can be realized when decreasing the power by controlling the secondary-side switching current. Case 3 is the DPS and TPS modulations with the unified transformer current. To simplify the elimination method, the compensation process focuses on the first half switching cycle in the next switching period [10]. But as mentioned in [5], in different modulation strategies, the minimum required inductor currents to realize ZVS are different. By unifying the switching current for the primary-side ZVS, the ZVS current setting could be higher than the optimal value inducing a slightly higher switching current or rms current. But the difference between the unified current and the optimal ZVS in certain modulation is small, which means it has little influence on steady-state performance.

IV. EXPERIMENT VERIFICATION

To validate the proposed modulation, experiments are conducted based on the test conditions shown in Table I, and results are shown in Fig. 7. Fig. 7(a) shows the experimental waveforms during a load transient when $V_{in} > nV_o$. Fig. 7(b) shows the experimental waveforms during a load transient when $V_{in} < nV_o$. Fig. 7(c) shows experimental waveforms during a load transient when $V_{in} = nV_o$. In all the experiments, the primary-side switches can realize ZVS no matter the load condition within the wide secondary-side voltage range. For the load current transient with the modulations switching between TPS and DPS, the proposed modulation strategy does not have the transformer current spike without considering any active compensation.

V. CONCLUSION

The transformer current spike is a common issue during a load transient in the DAB converter. The special compensation methods are developed in the previous research by adjusting certain switches' duty cycles to mitigate the current spike. This makes the compensation method much more complicated especially when using MPS modulation to improve the steady-state performance. In this letter, the elimination of transformer current spikes during load transients is considered when designing the steady-state modulation by unifying the transformer current in DPS and TPS modulation. In this case, there is no current spike fundamentally during the load transient. Also, the compensation

between SPS and other modulations can be simplified because of the unified transformer current. Meanwhile, the proposed modulation strategy utilizes the unified current to realize ZVS for the primary-side switches through the whole operation range. Finally, the performance of the proposed modulation is validated by experiments.

ACKNOWLEDGMENT

This work made use of the shared facilities of the Engineering Research Center Program of the National Science Foundation and the Department of Energy under NSF Award EEC-1041877.

REFERENCES

- [1] S. Shao et al., "Modeling and advanced control of dual-active-bridge dc–dc converters: A review," *IEEE Trans. Power Electron.*, vol. 37, no. 2, pp. 1524–1547, Feb. 2022, doi: [10.1109/TPEL.2021.3108157](https://doi.org/10.1109/TPEL.2021.3108157).
- [2] Y. Yan, H. Bai, A. Foote, and W. Wang, "Securing full-power-range zero-voltage switching in both steady-state and transient operations for a dual-active-bridge-based bidirectional electric vehicle charger," *IEEE Trans. Power Electron.*, vol. 35, no. 7, pp. 7506–7519, Jul. 2020, doi: [10.1109/TPEL.2019.2955896](https://doi.org/10.1109/TPEL.2019.2955896).
- [3] G. Xu, L. Li, X. Chen, Y. Liu, Y. Sun, and M. Su, "Optimized EPS control to achieve full load range ZVS with seamless transition for dual active bridge converters," *IEEE Trans. Ind. Electron.*, vol. 68, no. 9, pp. 8379–8390, Sep. 2021, doi: [10.1109/TIE.2020.3014562](https://doi.org/10.1109/TIE.2020.3014562).
- [4] J. Hu, S. Cui, and R. W. De Doncker, "Natural boundary transition and inherent dynamic control of a hybrid-mode-modulated dual-active-bridge converter," *IEEE Trans. Power Electron.*, vol. 37, no. 4, pp. 3865–3877, Apr. 2022, doi: [10.1109/TPEL.2021.3119903](https://doi.org/10.1109/TPEL.2021.3119903).
- [5] Y. Yan, H. Gui, and H. Bai, "Complete ZVS analysis in dual active bridge," *IEEE Trans. Power Electron.*, vol. 36, no. 2, pp. 1247–1252, Feb. 2021, doi: [10.1109/TPEL.2020.3011470](https://doi.org/10.1109/TPEL.2020.3011470).
- [6] X. Huang et al., "Comprehensive analysis and improvement methods of noise immunity of desat protection for high voltage SiC MOSFETs with high dv/dt," *IEEE Open J. Power Electron.*, vol. 3, pp. 36–50, 2022, doi: [10.1109/OJPEL.2021.3134498](https://doi.org/10.1109/OJPEL.2021.3134498).
- [7] B. Zhao, Q. Song, W. Liu, and Y. Zhao, "Transient dc bias and current impact effects of high-frequency-isolated bidirectional dc–dc converter in practice," *IEEE Trans. Power Electron.*, vol. 31, no. 4, pp. 3203–3216, Apr. 2016, doi: [10.1109/TPEL.2015.2445831](https://doi.org/10.1109/TPEL.2015.2445831).
- [8] S. Mu, Z. Guo, and Y. Luo, "Universal modulation scheme to suppress transient dc bias current in dual active bridge converters," *IEEE Trans. Power Electron.*, vol. 37, no. 2, pp. 1322–1333, Feb. 2022, doi: [10.1109/TPEL.2021.3104628](https://doi.org/10.1109/TPEL.2021.3104628).
- [9] N. Hou, Y. Li, Z. Quan, Y. W. Li, and A. Zhou, "Unified fast-dynamic direct-current control scheme for intermediary inductive ac-link isolated dc–dc converters," *IEEE Open J. Power Electron.*, vol. 2, pp. 383–400, 2021, doi: [10.1109/OJPEL.2021.3085863](https://doi.org/10.1109/OJPEL.2021.3085863).
- [10] J. Hu, S. Cui, D. V. D. Hoff, and R. W. De Doncker, "Generic dynamic phase-shift control for bidirectional dual-active bridge converters," *IEEE Trans. Power Electron.*, vol. 36, no. 6, pp. 6197–6202, Jun. 2021, doi: [10.1109/TPEL.2020.3039348](https://doi.org/10.1109/TPEL.2020.3039348).
- [11] S. Wei, D. Mou, W. Wen, Z. Zhao, and K. Li, "Transient dc bias and universal dynamic modulation of multiactive bridge converters," *IEEE Trans. Power Electron.*, vol. 37, no. 10, pp. 11516–11522, Oct. 2022, doi: [10.1109/TPEL.2022.3175320](https://doi.org/10.1109/TPEL.2022.3175320).
- [12] F. Krismer, S. Round, and J. W. Kolar, "Performance optimization of a high current dual active bridge with a wide operating voltage range," in *Proc. IEEE 37th Power Electron. Specialists Conf.*, 2006, pp. 1–7, doi: [10.1109/pesc.2006.1712096](https://doi.org/10.1109/pesc.2006.1712096).